Title	Directional Multiport Ambient RF Energy-Harvesting System for the Internet of Things
Authors	Shen, Shanpu; Zhang, Yujie; Chiu, Chi-Yuk; Murch, Ross
Source	IEEE Internet of Things Journal, v. 8, (7), April 2021, article number 9233414, P, p. 5850-5865
Version	Accepted Version
DOI	10.1109/JIOT.2020.3032435
Publisher	IEEE
Copyright	© 2020 IEEE. Personal use of this material is permitted. Permission from IEEE must be obtained for all other uses, in any current or future media, including reprinting/republishing this material for advertising or promotional purposes, creating new collective works, for resale or redistribution to servers or lists, or reuse of any copyrighted component of this work in other works.

Directional Multiport Ambient RF Energy Harvesting System for the Internet of Things

Shanpu Shen, *Member, IEEE,* Yujie Zhang, *Student Member, IEEE,*
Chi-Yuk Chiu, *Senior Member, IEEE,* and Ross Murch, *Fellow, IEEE*

***Abstract*—Ambient radio frequency (RF) energy harvesting can extract energy from RF signals in the ambient environment and has potential for applications in the Internet of Things. However, the power density of the ambient RF energy is low and therefore methods to maximize the average *output dc power* are required. In this work we show that average *output dc power* in ambient RF energy harvesting is nonlinearly dependent on antenna directivity and linearly dependent on antenna port number. To maximize average *output dc power* it is therefore necessary to utilize directional multiport rectennas. To demonstrate the enhancements possible, the design for a directional 4-port pixel patch rectenna system to harvest ambient RF energy from the GSM-1800 frequency band is provided. The design has an average antenna size for each port of $0.3\lambda \times 0.3\lambda$, and realized gains of 5.5 dBi. Measurement results show that the proposed rectenna can increase average output dc power by up to 6.2 dB and 4.5 dB compared to omni-directional and directional single-port rectenna designs of similar size, respectively. Measurement in a real ambient environment is also conducted, showing that the proposed rectenna can achieve an output dc power of 11.2 μW which is five times higher than the two reference rectennas.**

***Index Terms*—Directional, energy harvesting, multiport, pixel antenna, random radio-frequency (RF) field, rectenna, rectifier.**

I. Introduction

AMBIENT radio frequency (RF) energy harvesting is based on using rectifying antennas (rectenna) to extract energy from RF signals in the ambient environment [1]. It has the potential for alleviating the need for battery replacement or recharging in applications involving the Internet of Things (IoT) [2], [3]. Compared with solar [4], thermal [5], and other energy harvesting technologies [6], ambient RF energy harvesting has the advantage that it can provide mobility, operate without light, and be embedded in walls. However, as shown in various RF surveys [7], the power density of the ambient RF energy is extremely low, which limits the output direct current (dc) power of a rectenna. Therefore, the challenge of ambient RF energy harvesting is to maximize the output dc power.

To overcome the challenge, using multi-band rectennas have been proposed to increase the output dc power [8]. Compared with single-band rectennas which only harvest RF energy from single frequency band such as GSM-900 [7], GSM-1800 [7], 3G [7], LTE [9], AM [10], DTV [11], and WiFi [12], multi-band rectennas fully leverage the available ambient RF energy distributed at different frequency bands. Therefore dual-band [13]-[16], triple-band [17], [18], quad-band [19], hexa-band [20], and broadband rectennas [21], [22] have been designed to increase the output dc power.

Using multiple rectennas provides another possibility for increasing the output dc power. Two-dimensional (2-D) [23], [24] and three-dimensional (3-D) [25] uniform rectenna arrays are the most straightforward approach for implementing multiple rectenna systems, however they have a drawback that the overall antenna size is increased which makes the multiple rectenna system bulky. To reduce the overall antenna size, we face the challenge that generally high mutual coupling exists in a compact multiple antenna configuration [26]. The high mutual coupling will decrease the RF power received by multiple antennas. To compensate for mutual coupling, various impedance matching techniques have been proposed [27], however the matching comes at the cost of insertion loss and increased circuit complexity.

Multiport antennas, widely used in multiple-input multiple-output (MIMO) communication systems, have been designed with low mutual coupling for a compact and portable configuration. These multiport antennas have recently been utilized for ambient RF energy harvesting to increase the output dc power without increasing antenna size. For example, a dual-port triple-band L-probe microstrip patch rectenna [17], a 4-port dual-polarized dipole rectenna [28], and multiport pixel antennas with optimized RF power reception [29], [30] have been demonstrated. To implement multiport antennas, polarization, spatial, and angular diversities can be leveraged. Polarization diversity [31]-[33] can be exploited to harvest the ambient RF energy distributed in different polarizations. Spatial diversity [28], [34] and angular diversity [17], [29], [35], [36] can also be exploited to achieve wide spatial and angular coverage to harvest energy from different spatial and angular positions.

Combining the harvested energy from multiport antennas is an important issue and the advantages of RF and dc combining have been discussed previously [37]. It is concluded that dc combining might be more suitable for ambient RF energy harvesting because it can have a broad beamwidth with high gain for receiving RF signals from arbitrary directions. In addition, hybrid combining [38], [39] has been proposed to jointly leverage the benefits of RF combining and dc

Manuscript received; This work was supported by the Hong Kong Research Grants Council under Grant 16207314. *(Corresponding author: Shanpu Shen.)*

S. Shen, Y. Zhang and C. Y. Chiu are with the Department of Electronic and Computer Engineering, The Hong Kong University of Science and Technology, Clear Water Bay, Kowloon, Hong Kong, China. (email: sshenaa@connect.ust.hk).

R. Murch is with the Department of Electronic and Computer Engineering and the Institute of Advanced Study, The Hong Kong University of Science and Technology, Clear Water Bay, Kowloon, Hong Kong, China.

combining. Other techniques to improve the performance of RF energy harvesting systems include using reconfigurable RF energy harvester [40], hybrid RF-solar energy harvesting [41], and electrically small rectenna [42].

In this paper, we study the maximization of the average *output dc power* of multiport rectenna systems. The impact of increasing the number of antenna ports and/or increasing antenna directivity on the average output dc power is analyzed, both theoretically and numerically. Motivated by the findings in the study, we design, prototype, and experimentally validate a directional multiport rectenna system design for ambient RF energy harvesting that performs better than other rectenna designs. The contributions of this paper are summarized as follows:

1) We show that the average output direct current power increases nonlinearly with the antenna directivity and increases linearly with the number of antenna ports through analysis and numerical simulation. We also show that the benefit of antenna directivity is weak at high power density.

2) Motivated by the findings, we design a novel directional multiport rectenna system to maximize the average output dc power. It operates at the downlink channel of the GSM-1800 frequency band and consists of a compact 4-port pixel patch antenna, four single series diode rectifiers, and parallel dc combining. The proposed 4-port pixel patch antenna has an average antenna size of each antenna port of $0.3\lambda \times 0.3\lambda$ (λ refers to the free space wavelength) with the isolation between antenna ports greater than 10 dB and realized gain of 5.5 dBi for each port.

3) We demonstrate the approach with experimental results and provide comparisons with conventional omni-directional single-port monopole rectenna and directional single-port patch rectenna. Compared with the monopole rectenna and the patch rectenna, our proposed rectenna can increase the average output dc power by up to 6.2 dB and 4.5 dB, respectively. We also measure the proposed rectenna and the two reference rectennas in a real ambient environment. The measurement results show that the monopole rectenna and the patch rectenna can achieve output dc power of 1.4 μW and 2.1 μW, respectively, while the proposed rectenna can achieve an output dc power of 11.2 μW which is five times higher than that of the two reference rectennas. Therefore, using the proposed directional multiport rectenna system can maximize average output dc power to overcome the challenge of low power densities in ambient RF energy harvesting.

This work is different from previous work [29], [34] in that 1) the nonlinearity of the rectifier was not considered in [29], [34] while this work fully considers the nonlinearity, and 2) maximizing average output dc power was not considered in [29], [34] while this work provides a thorough investigation.

It is also worthwhile to compare our proposed rectenna design with the recent rectenna designs based on tightly coupled antennas (TCA) [43] and on metasurfaces [44]. There are three differences between those two work and ours that we would like to highlight: 1) The rectennas based on TCA and metasurfaces both use infinite periodic unit cells so that they are for large-scale rectenna applications. Our proposed rectenna focuses on designing efficient multiport rectenna in a compact antenna area. 2) The rectennas based on TCA and metasurfaces can both absorb incident RF waves from the broadside direction with high absorbing efficiency. They have less absorbing efficiency for other incident directions, so they are more suitable for wireless power transfer where the incident direction is known. Our proposed rectenna is designed for ambient RF energy harvesting and fully considers the unknown and random incident direction of ambient RF energy to maximize the average output dc power. 3) The rectennas based on TCA and metasurfaces both focus on high input RF power above 9 dBm and is again more suitable for wireless power transfer. Our proposed rectenna is designed for low input RF power below -10 dBm where the rectifier nonlinearity has been fully leveraged to increase the output dc power.

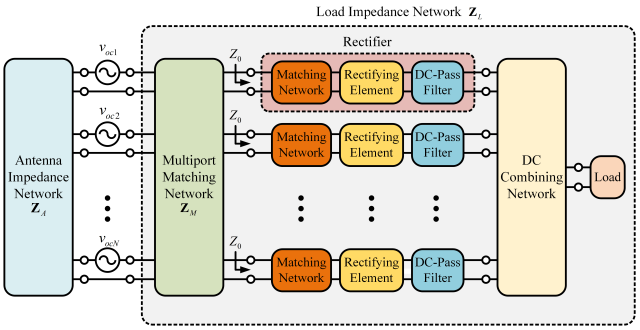

Fig. 1. The ambient RF energy harvesting system with an N-port rectenna.

Organization: In Section II, we analyze the maximization of average received RF power and average output dc power of multiport rectenna systems in ambient RF environments. In Section III, we numerically simulate the average received RF power and average output dc power to verify the analysis. In Section IV, we describe the design and optimization of a directional 4-port pixel patch rectenna system. In Section V, we provide measurement results and comparisons to show the effectiveness of the design. Section VI concludes the paper.

II. Multiport Rectenna System

A. System Model

Consider an RF energy harvesting system with an N-port rectenna immersed in an ambient RF field as shown in Fig. 1. The N-port antenna is modeled by an $N \times N$ antenna impedance matrix $\mathbf{Z}_A$. The open-circuit voltage across the ith antenna port is denoted as $v_{\text{oc}i}$ $(i = 1, \ldots, N)$ and they are grouped into an N-dimensional vector referred to as the open-circuit voltage vector, $\mathbf{v}_{\text{oc}} = [v_{\text{oc}1}, v_{\text{oc}2}, ..., v_{\text{oc}N}]^T$. A $2N \times 2N$ multiport matching decoupling network $\mathbf{Z}_M$ is inserted between the antenna impedance matrix $\mathbf{Z}_A$ and N rectifiers, whose input impedance is the standard load, $Z_0 = 50\ \Omega$. Each rectifier consists of a matching network which matches the rectifier to Z_0, a rectifying element such as a diode, and a dc pass filter. The dc power output of the N rectifiers are combined through a dc combining network so that the total output dc power can be extracted from the load. The multiport matching network $\mathbf{Z}_M$, the N rectifiers with dc combining network, and the load can be viewed as an N-port load impedance $\mathbf{Z}_L$ for simplification [27].

RF energy in the ambient environment is modeled as a random RF field so that the open-circuit voltage across the ith port v_{oci}, the RF power received by the ith port P_{RF}^{i}, and the total received RF power $P_{\mathrm{RF}}=\sum_{i=1}^{N}P_{\mathrm{RF}}^{i}$ are all random variables. Hence, we consider the ensemble averaged total RF power received by the N-port antenna, which is given by [27]

$$\mathrm{E}\left[P_{\mathrm{RF}}\right]=\mathrm{Tr}\left(\mathbf{R}_{L}\left(\mathbf{Z}_{A}+\mathbf{Z}_{L}\right)^{-1}\mathbf{C}\left(\mathbf{Z}_{A}+\mathbf{Z}_{L}\right)^{-H}\right) \quad (1)$$

where $\mathrm{E}\left[\cdot\right]$ is expectation, $\mathrm{Tr}\left(\cdot\right)$ is trace, $\mathbf{R}_{L}=\mathrm{Re}\left(\mathbf{Z}_{L}\right)$ denotes the load resistance matrix (where $\mathrm{Re}\left(\cdot\right)$ is the real part), and $\mathbf{C}=\mathrm{E}\left[\mathbf{v}_{\mathrm{oc}}\mathbf{v}_{\mathrm{oc}}^{H}\right]$ is the correlation matrix of $\mathbf{v}_{\mathrm{oc}}$.

We assume that the random RF field has uncorrelated equally likely polarizations (that is the ambient RF energy is uniformly randomly distributed in orthogonal polarizations) and each polarization is spatially uncorrelated [45] so its power angular spectrum (PAS) can be written as $S\left(\Omega\right)\mathbf{I}_{2}$ where $\Omega=\left(\theta,\phi\right)$ denotes spatial angle with θ and ϕ representing the elevation and azimuth angles in spherical coordinates and $\mathbf{I}_{2}$ is the 2×2 identity matrix. The (i,j)th element $\left[\mathbf{C}\right]_{ij}$ can then be written as [45]

$$\left[\mathbf{C}\right]_{ij}=\mathrm{E}\left[v_{oci}v_{ocj}^{*}\right]=\int S(\Omega)\mathbf{h}_{i}\left(\Omega\right)\cdot\mathbf{h}_{j}^{*}\left(\Omega\right)\mathrm{d}\Omega \quad (2)$$

where * refers to complex conjugate and $\mathbf{h}_{i}\left(\Omega\right)$ is the antenna height of the ith port and is expressed as [46]

$$\mathbf{h}_{i}\left(\Omega\right)=\frac{\lambda}{j}\sqrt{\frac{\left[\mathbf{R}_{A}\right]_{ii}e_{i}D_{i}}{\pi Z_{\eta}}}\mathbf{E}_{i}\left(\Omega\right) \quad (3)$$

where λ, j, and Z_{η} denote the wavelength, imaginary unit, and intrinsic impedance of free space, respectively. $\mathbf{R}_{A}=\mathrm{Re}\left(\mathbf{Z}_{A}\right)$ is the antenna resistance matrix and $\left[\mathbf{R}_{A}\right]_{ii}$ denotes its (i,i)th element representing the self-resistance of the ith port. $\mathbf{E}_{i}\left(\Omega\right)$ denotes the normalized electric far-field pattern of the ith port with other ports open-circuited (i.e. $\left|\mathbf{E}_{i}\left(\Omega\right)\right|_{\max}=1$). D_{i} and e_{i} denote the directivity and radiation efficiency of the ith port with other ports open-circuited, respectively. Directivity is expressed as

$$D_{i}=\frac{4\pi}{\int\left|\mathbf{E}_{i}\left(\Omega\right)\right|^{2}\mathrm{d}\Omega}. \quad (4)$$

Substituting (4) into (3) and making use of (2), the self correlation of the open-circuit voltage across the ith port is given by

$$\left[\mathbf{C}\right]_{ii}=\frac{4\lambda^{2}\left[\mathbf{R}_{A}\right]_{ii}e_{i}}{Z_{\eta}}\cdot\frac{\int S(\Omega)\left|\mathbf{E}_{i}\left(\Omega\right)\right|^{2}\mathrm{d}\Omega}{\int\left|\mathbf{E}_{i}\left(\Omega\right)\right|^{2}\mathrm{d}\Omega}. \quad (5)$$

Multiport conjugate matching (MCM) ($\mathbf{Z}_{L}=\mathbf{Z}_{A}^{H}$) provides the maximum average received RF power [26], which can be written as $\mathrm{E}\left[P_{\mathrm{RF}}\right]_{\max}=\frac{1}{4}\mathrm{Tr}\left(\mathbf{C}\mathbf{R}_{A}^{-1}\right)$. However, a disadvantage of MCM is that $\mathbf{Z}_{L}=\mathbf{Z}_{A}^{H}$ in this configuration is not a diagonal matrix. Therefore $\mathbf{Z}_{M}$ becomes intricate and has narrow bandwidth, with high insertion loss [26].

An alternative method to reduce the multiport conjugate matching problem is to utilize antennas with good isolation so that a multiport matching network $\mathbf{Z}_{M}$ is not required. Compact multiport antennas developed for MIMO communication systems fall into this category and typically their reflection coefficients S_{ii} and couplings S_{ij} are less than -10 dB. Both $\mathbf{Z}_{A}$ and $\mathbf{C}$ can then be approximated as diagonal matrices with $\mathbf{Z}_{A}=Z_{0}\mathbf{I}_{N}$ where $\mathbf{I}_{N}$ denotes the $N\times N$ identity matrix. Therefore, the maximum average RF power received by this type of multiport antenna can be simplified as $\mathrm{E}\left[P_{\mathrm{RF}}\right]_{\max}=\frac{1}{4}\sum_{i=1}^{N}\left[\mathbf{C}\right]_{ii}/\left[\mathbf{R}_{A}\right]_{ii}$. Making use of (5), we then can rewrite $\mathrm{E}\left[P_{\mathrm{RF}}\right]_{\max}$ as

$$\mathrm{E}\left[P_{\mathrm{RF}}\right]_{\max}=\frac{\lambda^{2}}{Z_{\eta}}\sum_{i=1}^{N}e_{i}\frac{\int S\left(\Omega\right)\left|\mathbf{E}_{i}\left(\Omega\right)\right|^{2}\mathrm{d}\Omega}{\int\left|\mathbf{E}_{i}\left(\Omega\right)\right|^{2}\mathrm{d}\Omega}. \quad (6)$$

Now, we can see that $\mathrm{E}\left[P_{\mathrm{RF}}\right]_{\max}$ depends on $\left|\mathbf{E}_{i}\left(\Omega\right)\right|$.

B. Maximization of Average Received RF Power

We first maximize average received RF power as an intermediate step towards maximizing average *output dc power*. We separate out terms under the integrals in the numerator and denominator in (6) and use the straightforward inequality

$$\int S(\Omega)\left|\mathbf{E}_{i}\left(\Omega\right)\right|^{2}\mathrm{d}\Omega\leq S_{0}\int\left|\mathbf{E}_{i}\left(\Omega\right)\right|^{2}\mathrm{d}\Omega \quad (7)$$

where $S_{0}=\max\left(S(\Omega)\right)$. Therefore an upper bound on the maximum average received RF power is

$$\mathrm{E}\left[P_{\mathrm{RF}}\right]_{\max}\leq\frac{\lambda^{2}S_{0}}{Z_{\eta}}\sum_{i=1}^{N}e_{i}. \quad (8)$$

In ambient RF environments we can assume that

$$S\left(\Omega\right)=\begin{cases}S_{0} & ,\Omega\in\Omega_{\mathrm{inc}}\\ 0 & ,\Omega\in\text{elsewhere}\end{cases} \quad (9)$$

where the power angular spectrum is constant, S_{0}, over some set of angles Ω_{inc} and zero elsewhere (for example the situation when PAS is constant over a sector of elevation angles ($\theta_{l}\leq\theta\leq\theta_{u}$) and all azimuth angles ($0\leq\phi\leq2\pi$) where θ_{l} and θ_{u} are the lower and upper bounds of the sector). That is the ambient RF energy could appear from different angles within Ω_{inc}. The maximum average received RF power reaches the upper bound in (8) when the following condition is satisfied

$$\left|\mathbf{E}_{i}\left(\Omega\right)\right|=\begin{cases}(0,1] & ,\Omega\in\Omega_{\mathrm{inc}}^{\mathrm{sub}}\\ 0 & ,\Omega\in\text{elsewhere}\end{cases} \quad (10)$$

where $\Omega_{\mathrm{inc}}^{\mathrm{sub}}$ is any subset of Ω_{inc} and $(0,1]$ is the range $0<\left|\mathbf{E}_{i}\left(\Omega\right)\right|\leq1$.

From (7)-(10) it is concluded that 1) the average total received RF power increases linearly with the number of antenna ports no matter whether the multiple antenna ports arise from polarization, spatial, or angular diversity, and 2) it does not depend on directivity. That is any directional antenna whose $\left|\mathbf{E}_{i}\left(\Omega\right)\right|$ satisfying (10) with directivity given by $D_{i}=4\pi/\int\left|\mathbf{E}_{i}\left(\Omega\right)\right|^{2}\mathrm{d}\Omega$ would maximize the received RF power.

To highlight this further, for the special case of 3-D uniform PAS, i.e. $S(\Omega)=S_{0}$, average received RF power reaches the bound in (8) no matter its directivity since (10) is always satisfied. More generally for PAS defined by (9) and normalized far-field antenna patterns satisfying (10), average RF power

received by multiport antennas with good isolation does not depend on antenna directivity and it increases linearly with the number of antenna ports.

C. Maximization of Average Output DC Power

Average *output dc power* depends on both the average received RF power and the nonlinear rectification process. It is the key overall parameter we wish to maximize in ambient RF energy harvesting. It is very important to distinguish the difference between the average received RF power and the average output dc power, as the former is the power input into the rectifier. Specifically, the RF power received by the ith antenna port P_{RF}^{i} is input to the ith rectifier so that the output dc power of the ith rectifier, denoted as P_{DC}^{i}, is given by

$$P_{\mathrm{DC}}^{i} = P_{\mathrm{RF}}^{i}\eta\left(P_{\mathrm{RF}}^{i}\right) \tag{11}$$

where $\eta\left(P_{\mathrm{RF}}^{i}\right)$ is a nonlinear function that refers to the RF-to-dc efficiency of the ith rectifier at the input RF power P_{RF}^{i}. We assume all the rectifiers are identical without loss of generality. Therefore, the total output dc power, P_{DC}, is given by

$$P_{\mathrm{DC}} = e_d \sum_{i=1}^{N} P_{\mathrm{DC}}^{i} = e_d \sum_{i=1}^{N} P_{\mathrm{RF}}^{i}\eta\left(P_{\mathrm{RF}}^{i}\right) \tag{12}$$

where e_d is the efficiency of the dc combining circuit. P_{DC}^{i} and P_{DC} are random variables since P_{RF}^{i} is a random variable. Hence, we are interested in the ensemble averaged total output dc power $\mathrm{E}\left[P_{\mathrm{DC}}\right]$.

$\eta\left(P_{\mathrm{RF}}^{i}\right)$ plays a crucial role in analyzing $\mathrm{E}\left[P_{\mathrm{DC}}\right]$. If we consider a linear rectifier model which assumes that the RF-to-dc efficiency is a constant, i.e. $\eta\left(P_{\mathrm{RF}}^{i}\right) = \eta$, then we have that $P_{\mathrm{DC}} = e_d\eta P_{\mathrm{RF}}$ and $\mathrm{E}\left[P_{\mathrm{DC}}\right] = e_d\eta\mathrm{E}\left[P_{\mathrm{RF}}\right]$, which indicates that the average output dc power does not depend on directivity similarly to the result in Section II.B. However, a rectifier is a nonlinear circuit element where $\eta\left(P_{\mathrm{RF}}^{i}\right)$ increases with P_{RF}^{i} until a turning point, denoted as $P_{\mathrm{RF}}^{\eta\max}$, and after $P_{\mathrm{RF}}^{\eta\max}$ $\eta\left(P_{\mathrm{RF}}^{i}\right)$ decreases because of the diode breakdown effect. Therefore, the nonlinear $\eta\left(P_{\mathrm{RF}}^{i}\right)$ affects the expression of $\mathrm{E}\left[P_{\mathrm{DC}}\right]$ so that it cannot be ignored.

To find $\mathrm{E}\left[P_{\mathrm{DC}}\right]$, we need to know the instantaneous received RF power at each antenna port P_{RF}^{i}, which requires knowing the instantaneous incident electric field (the realization of the random RF field). However, the instantaneous electric field distribution is an Ergodic stochastic process and we only know its ensemble average from its PAS. Therefore there are many instantaneous electric field distributions in time and angular space that will provide the same PAS. We consider two extreme instantaneous incident electric field scenarios which provide 3-D uniform PAS, $S(\Omega) = S_0$.

We first consider an electric field which is completely uniformly distributed in all angular directions each with a random phase. Its instantaneous incident power density per steradian at any angle is S_0, providing a 3-D uniform PAS. We denote this incident electric field scenario as $\mathbf{E}_{\mathrm{inc}}^{\mathrm{Rayleigh}}$ since it is the conventional definition for a Rayleigh fading channel. For the scenario $\mathbf{E}_{\mathrm{inc}}^{\mathrm{Rayleigh}}$, the instantaneous received RF power P_{RF}^{i} follows an exponential distribution, denoted as $P_{\mathrm{RF}}^{i} \sim \mathrm{Exp}\left(\mathrm{E}\left[P_{\mathrm{RF}}^{i}\right]^{-1}\right)$. It has been shown in Section II.B that antenna directivity has no effect on the average received RF power $\mathrm{E}\left[P_{\mathrm{RF}}^{i}\right]$, so the distribution of P_{RF}^{i} does not depend on antenna directivity. As a result, in this scenario antenna directivity also has no effect on the instantaneous output dc power P_{DC}^{i} and the average output dc power $\mathrm{E}\left[P_{\mathrm{DC}}\right]$.

In the second scenario, a single incident plane wave with random phase and arriving with random uniformly distributed angles over 4π spatial angles in time will also provide a 3-D uniform PAS. The power density of the plane wave is $4\pi S_0/Z_\eta$ and also corresponds to 3-D uniform PAS with S_0 power density per steradian. We denote this incident electric field scenario as $\mathbf{E}_{\mathrm{inc}}^{\mathrm{Beam}}$. For the scenario $\mathbf{E}_{\mathrm{inc}}^{\mathrm{Beam}}$, antenna directivity will have a significant effect on the average output dc power $\mathrm{E}\left[P_{\mathrm{DC}}\right]$ because the instantaneous received RF power changes significantly with the antenna directivity.

To obtain insight into the effects of antenna directivity on the average output dc power $\mathrm{E}\left[P_{\mathrm{DC}}\right]$, we need to find the closed-form expression of $\mathrm{E}\left[P_{\mathrm{DC}}\right]$. In the scenario $\mathbf{E}_{\mathrm{inc}}^{\mathrm{Beam}}$, the plane wave is arriving with random uniformly distributed angles over 4π spatial angles, so the average output dc power of the ith rectifier is given by

$$\mathrm{E}\left[P_{\mathrm{DC}}^{i}\right] = \int P_{\mathrm{RF}}^{i}\left(\Omega\right)\eta\left(P_{\mathrm{RF}}^{i}\left(\Omega\right)\right)\frac{1}{4\pi}\mathrm{d}\Omega \tag{13}$$

where $P_{\mathrm{RF}}^{i}\left(\Omega\right)$ denotes the RF power received by the ith antenna port given a single incident plane wave with power density $4\pi S_0/Z_\eta$ arriving from Ω. According to [46], $P_{\mathrm{RF}}^{i}\left(\Omega\right)$ can be found by

$$P_{\mathrm{RF}}^{i}\left(\Omega\right) = \frac{\lambda^2}{4\pi}\cdot e_i D_i\left(\Omega\right)\cdot\frac{4\pi S_0}{Z_\eta} \tag{14}$$

where $D_i\left(\Omega\right)$ denotes the directivity function of the ith antenna port. Unfortunately, it is difficult to find the closed-form expressions of $\mathrm{E}\left[P_{\mathrm{DC}}^{i}\right]$ and $\mathrm{E}\left[P_{\mathrm{DC}}\right]$ because there is no closed-form solution for $\eta\left(P_{\mathrm{RF}}^{i}\right)$.

To overcome the challenge for finding the closed-form expressions of $\mathrm{E}\left[P_{\mathrm{DC}}\right]$, we consider antennas that have an idealized normalized far-field radiation pattern given by

$$\left|\mathbf{E}_i\left(\Omega\right)\right| = \begin{cases} 1 & ,\Omega \in \Omega_{\mathrm{main}}^{i} \\ 0 & ,\Omega \in \Omega_{\mathrm{side}}^{i} \end{cases} \tag{15}$$

where $\Omega_{\mathrm{main}}^{i}$ and $\Omega_{\mathrm{side}}^{i}$ are spatial angle sets representing the main and side lobes of the ith antenna radiation pattern, respectively. Such idealized radiation pattern approximates a realistic radiation pattern by assuming all the radiated power is uniformly distributed within the main lobe of the pattern. Accordingly, the directivity function of the ith antenna port can be written as

$$D_i\left(\Omega\right) = \begin{cases} D_i & ,\Omega \in \Omega_{\mathrm{main}}^{i} \\ 0 & ,\Omega \in \Omega_{\mathrm{side}}^{i} \end{cases} \tag{16}$$

where $D_i = 4\pi/\int_{\Omega_{\mathrm{main}}^{i}}\mathrm{d}\Omega$ is found from antenna directivity (4). Hence, $P_{\mathrm{RF}}^{i}\left(\Omega\right)$ can be written as

$$P_{\mathrm{RF}}^{i}\left(\Omega\right) = \begin{cases} \frac{\lambda^2}{4\pi}\cdot e_i D_i\cdot\frac{4\pi S_0}{Z_\eta} & ,\Omega \in \Omega_{\mathrm{main}}^{i} \\ 0 & ,\Omega \in \Omega_{\mathrm{side}}^{i} \end{cases}. \tag{17}$$

Using (13), $\mathrm{E}\left[P_{\mathrm{DC}}^{i}\right]$ can be found by

$$\mathrm{E}\left[P_{\mathrm{DC}}^{i}\right]=\frac{\lambda^{2}S_{0}e_{i}}{Z_{\eta}}\eta\left(\frac{\lambda^{2}S_{0}e_{i}}{Z_{\eta}}D_{i}\right) \tag{18}$$

which increases with D_i as long as $\lambda^2 S_0 e_i D_i/Z_\eta$ is lower than $P_{\mathrm{RF}}^{\eta\max}$, which is the input RF power achieving the maximum RF-to-dc efficiency. When $\lambda^2 S_0 e_i D_i/Z_\eta$ is higher than $P_{\mathrm{RF}}^{\eta\max}$, $\mathrm{E}\left[P_{\mathrm{DC}}^{i}\right]$ will decrease with D_i due to the breakdown effect of the diode. However, this case is not probable since the power density of ambient RF energy is very low. The average total output dc power of the multiport rectenna is given by

$$\mathrm{E}\left[P_{\mathrm{DC}}\right]=\frac{e_d\lambda^{2}S_{0}}{Z_{\eta}}\sum_{i=1}^{N}e_{i}\eta\left(\frac{\lambda^{2}S_{0}e_{i}}{Z_{\eta}}D_{i}\right). \tag{19}$$

It can be concluded that total average output dc power 1) increases nonlinearly with the antenna directivity of each port which is related to the nonlinear RF-to-dc efficiency versus input power characteristic of the rectifier and 2) increases linearly with the number of antenna ports no matter whether the multiple antenna ports arise from polarization, spatial, or angular diversity.

It should be noted that the theoretical result (19) based on an idealized radiation pattern is used to help investigate the impact of antenna directivity on the average output dc power, instead of accurately predicting the average output dc power. More generally for realistic radiation patterns, (19) would represent an upper bound to the improvement in average output dc power. These conclusions also hold for PAS defined by (9).

In practice the incident electric field is between the $\mathbf{E}_{\mathrm{inc}}^{\mathrm{Rayleigh}}$ and $\mathbf{E}_{\mathrm{inc}}^{\mathrm{Beam}}$scenarios. The practical incident electric field often has a random beam like structure where incident power density at a particular time interval is higher in some directions than others. Therefore, given that antenna directivity does not affect the average output dc power in $\mathbf{E}_{\mathrm{inc}}^{\mathrm{Rayleigh}}$ scenario but it can boost the average output dc power in $\mathbf{E}_{\mathrm{inc}}^{\mathrm{Beam}}$ scenario (and also incident electric field having random beam like structure), it makes sense to increase the directivity of the antenna in ambient RF energy harvesting for all scenarios.

If we were also to assume that the incident plane is transient in time then even greater instantaneous power densities could be achieved and this has been exploited to boost the dc power by optimizing the waveform in wireless power transfer systems [47]. However our interest here is in the effect of the angular distribution of the instantaneous electric field on antenna design.

III. Numerical Simulation

To show that antenna directivity has no effect on the average received RF power and also quantify the effect of antenna directivity on the average output dc power under the $\mathbf{E}_{\mathrm{inc}}^{\mathrm{Beam}}$ scenario, we provide numerical simulations for the average received RF power and average output dc power for realistic antennas and a rectifier. The numerical simulations are performed by joint simulation in CST Microwave Studio and Advanced Design System (ADS). We focus on the single-port rectenna for harvesting RF energy from the downlink channel of GSM-1800 (1.8–1.88 GHz) band. For the purposes

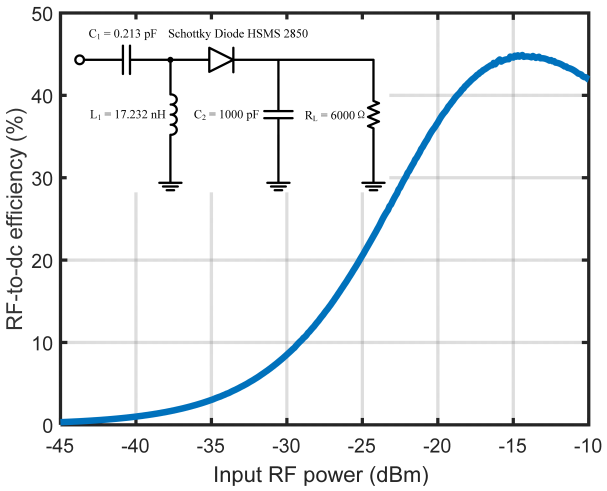

Fig. 2. Topology of the rectifier used in the numerical simulation and the simulated RF-to-dc efficiency versus input RF power at 1.8 GHz.

of revealing the effect of directivity we again assume that a single incident plane wave with power density of $4\pi S_0/Z_\eta$ is incident and the incident angle is uniformly distributed over 4π spatial angles in time. We achieve a realistic antenna directivity range by considering various antenna types ranging from monopole, loop, inverted-F, slot, patch, and finally Yagi antennas with 5, 9 and 12 elements, respectively. These were simulated using CST and provide gains of between 0 dBi (by including an ideal isotropic pattern) through to 14.5 dBi (for the 12 element Yagi) in the numerical simulations. A single series diode rectifier operating in the GSM-1800 frequency band is designed and considered in the numerical simulation as shown in Fig. 2. Its RF-to-dc efficiency simulated by ADS is also shown in Fig. 2, and it is used in the numerical simulation to find the output dc power.

The average received RF power (or average output dc power) is found by three steps: 1) generating multiple independent random incident spatial angles, 2) finding the received RF power (or output dc power) for each angle, and 3) averaging the received RF power (or output dc power) over all angles.

The average received RF power versus antenna directivity at different incident power densities based on the numerical simulation and the theoretical analysis (8) is provided in Fig. 3(a) and (b), respectively. We can find that the numerical result matches very well with the theoretical results. Both the theoretical and numerical results show that the average received RF power does not depend on antenna directivity no matter how large the power density is, which verifies the correctness of the theoretical analysis on the average received RF power. Besides, there is a small fluctuation of the average received RF power, less than 1.4 %, in Fig. 3(a). The fluctuation arises from using discretized radiation patterns. The incident spatial angle is a continuous random variable, but the radiation pattern simulated by CST is discretized, i.e. we only find the radiation pattern at $\theta = 0°, 1°, \ldots, 180°$ and $\phi = 0°, 1°, \ldots, 359°$. So, in step 2), the continuous angles are rounded to integers to approximately find its radiation pattern and then its received RF power, which causes the numerical

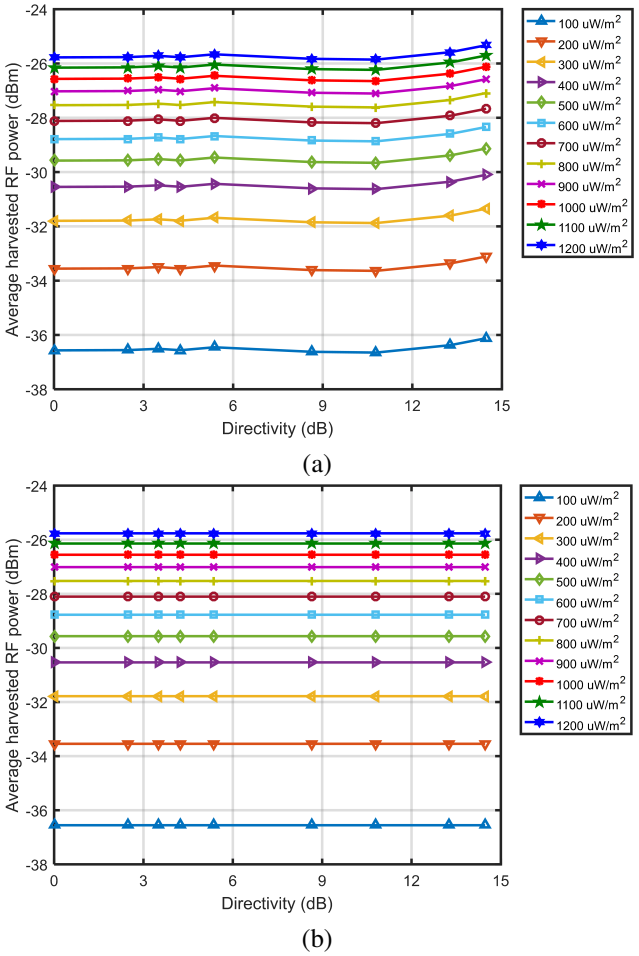

Fig. 3. Average received RF power versus antenna directivity at different incident wave power densities (a) based on the numerical simulation and (b) based on the theoretical analysis (8).

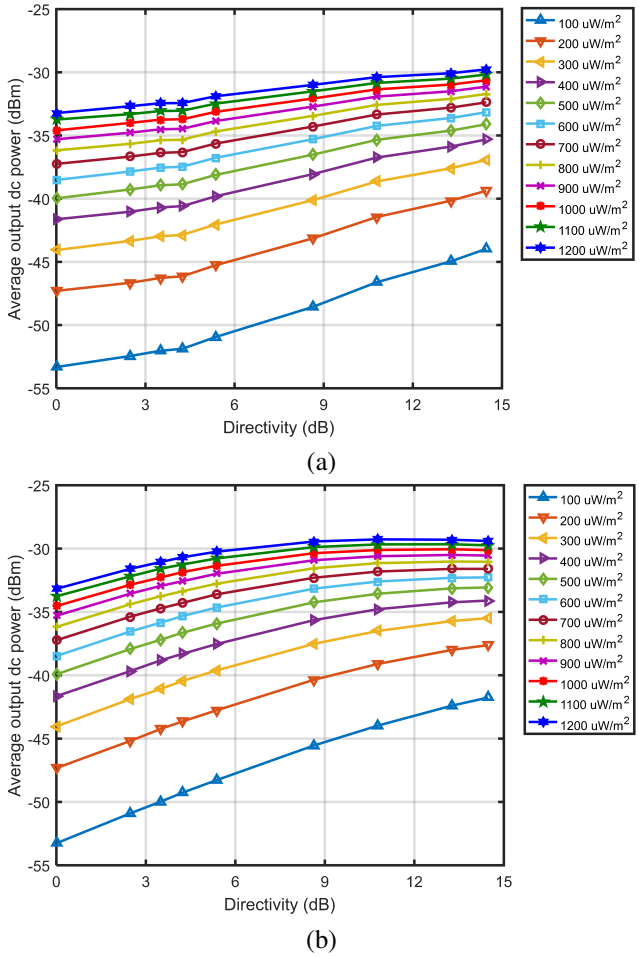

Fig. 4. Average output dc power versus antenna directivity at different incident wave power densities (a) based on the numerical simulation and (b) based on the theoretical analysis (19).

error and the fluctuation. Particularly, for an antenna with high directivity, the numerical error is relatively higher because its radiation pattern has a very narrow beam so that the pattern changes greatly even when the angle changes only 1°.

On the other hand, the average output dc power versus antenna directivity at different incident power densities based on the numerical simulation and the theoretical analysis (19) is provided in Fig. 4(a) and (b), respectively. The numerical and theoretical results do not exactly match because the numerical result is based on realistic radiation patterns while the theoretical result is based on idealized radiation patterns. Nevertheless, the numerical and theoretical results show the same trend that the average output dc power increases with antenna directivity, which verifies the correctness of the theoretical analysis on the average output dc power.

It is also worthwhile to quantify the increase of the average output dc power with antenna directivity. From Fig. 4(a), we can observe that the average output dc power increment between low and high gain antennas is large when the power density is low. Specifically, it can be deduced that when antenna directivity increases from 0 to 14.5 dBi, average output dc power increases by 9.35 dB for an incident power density of 100 $\mu\mathrm{W}/\mathrm{m}^2$. At a power density of 1200 $\mu\mathrm{W}/\mathrm{m}^2$ the increase is less at 3.46 dB. Considering the largest gradient of the lines in Fig. 4(a) (the 100 $\mu\mathrm{W}/\mathrm{m}^2$ line at around 9-14 dB), this implies that approximately a doubling of antenna directivity (3 dB) doubles the average output dc power (3 dB) at best. Therefore, antenna directivity has a significant effect on the average output dc power when the power density is low. However, this effect becomes weaker at higher incident power densities where the gradients of the lines in Fig. 4(a) are less due to the nonlinear RF-to-dc efficiency of the rectifier.

IV. Directional Multiport Ambient RF Energy Harvesting System Design

In this section, we provide a directional 4-port rectenna system design for ambient RF energy harvesting based on the analysis and simulation in Sections II and III. It consists of a 4-port microstrip pixel patch antenna, four single series diode rectifiers, and parallel dc combining.

A. Antenna Design

To design antennas that maximize average output dc power we should maximize the number of antenna ports and antenna directivity within a given volume. Doubling antenna area

roughly corresponds to doubling the number of antenna ports or doubling antenna directivity. However, the increase of average output dc power with antenna directivity is weak when the power density is high while the increase with the number of antenna ports is linear and independent on the power density. Hence, it is more beneficial to increase the number of antenna ports rather than the directivity as it is applicable across a wider range of power scenarios. Therefore, antenna port number maximization should take priority over directivity maximization.

The constraint of a fixed volume makes the maximization process difficult. In a fixed area or volume, the number of antenna ports can be increased by leveraging polarization, spatial, and angular diversities, however, the increase does not come without physical limits. Mutual coupling will increase as we add more antennas into the fixed volume limiting the total energy that can be harvested. On the other hand, there is also a physical limit for increasing antenna directivity given a fixed area or volume [46]. Therefore the design challenge is to squeeze as many compact antennas into the fixed area or volume with the lowest mutual coupling acceptable for energy harvesting while maximizing the directivity of individual antennas in the system. In addition, the radiation efficiency of each antenna port and the efficiency of the dc combining circuit should also be maximized for maximizing average output dc power according to (19). Optimization is therefore required in the antenna design process to achieve the best trade-off between the antenna port number and directivity so that a given volume can be fully utilized to maximize the average output dc power.

In the optimization approach adopted here we use the pixel antenna approach which can be broadly thought of as "programmable" or "software defined" antennas. The concept of pixel antennas is based on discretizing a radiation surface into small elements and connecting them through switches or hardwires [48], [49]. Given a mother structure such as a grid of pixels, different antenna characteristics including S-parameters [48] and radiation pattern [49] can be obtained by changing the connections between them so that we can achieve desired antenna features by optimizing the connection configuration. Applying the pixel antenna approach in the microstrip antenna design, we propose a 4-port microstrip pixel patch antenna design as shown in Fig. 5. The patch is discretized into a rectangular grid of 10 × 10 square pixels. The pixelized patch is printed on a Rogers 4003 (ϵ_r = 3.38) substrate having a thickness of 1.524 mm and thick air substrate is used to improve the radiation efficiency and bandwidth. It has four ports fed by disk-loaded probes to improve the bandwidth. Each pixel can connect to its neighboring pixels and there are $Q = 180$ possible hardwires. We use binary digits $x_q \in \{0, 1\}$ $(q = 1, 2, \ldots, Q)$ to represent the presence or absence of hardwires between pixels and group them into a vector $\mathbf{x} = [x_1, x_2, \ldots, x_Q]^T$ to describe the hardwire configuration. In total there are 2^Q combinations of $\mathbf{x}$ producing various distinct antenna characteristics. Therefore, we can evaluate a wide range of possible pixel patch antenna characteristics to find the optimum hardwire configuration for implementing the directional 4-port rectenna system.

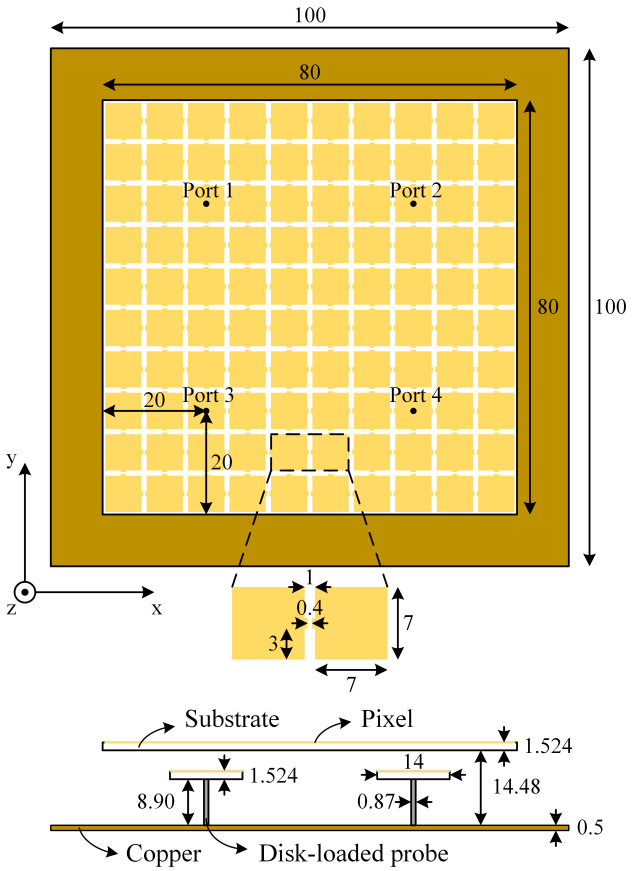

Fig. 5. Plan and elevation views of the 4-port microstrip pixel patch antenna (unit: mm).

Our pixel antenna design does not require any switches so that the complexity of antenna is not increased compared to other designs [43]. It should be noted that the hardwires used in the design are fixed in position and can be thought of as part of the antenna geometry and do not increase complexity any more than geometric features of other antennas. The key reason for using the pixel antenna design approach is that it provides a convenient method for optimizing directional multiport antenna but once optimized the antenna geometry is completely fixed.

We consider optimizing four objectives to achieve, 1) good impedance matching, 2) good port isolation, 3) high radiation efficiency, and 4) high antenna directivity, for average output dc power maximization. We combine the four objectives into a single objective based on the realized antenna gain found by the loaded-circuit radiation patterns. The *loaded-circuit radiation pattern* is defined as when one port is measured while the other ports are connected to 50 Ω. It should be distinguished from *open-circuit radiation pattern* which is defined as when one port is measured and the other ports are open-circuited. The two kinds of patterns can be related to each other through the antenna impedance matrix $\mathbf{Z}_A$. If there is no or low mutual coupling, the two kinds of patterns are approximately identical. However, multiport antennas typically have mutual coupling and therefore the kind of pattern measured needs to be carefully mentioned. In Section

II, we use the open-circuit radiation pattern $\mathbf{E}_i(\Omega)$ to find the correlation matrix $\mathbf{C} = \mathrm{E}\left[\mathbf{v}_{\mathrm{oc}}\mathbf{v}_{\mathrm{oc}}^H\right]$ and then analyze the average output dc power. However, herein we use the loaded-circuit radiation pattern to find the realized gain of each port. The benefit is that maximizing the realized antenna gain of each port simultaneously improves impedance matching, radiation efficiency, and directivity, and port isolation. For the 4-port pixel patch antenna with the hardwire configuration $\mathbf{x}$, we denote its realized antenna gain at the ith port at frequency f as $G_{\mathrm{real}}^i(\mathbf{x}, f)$. To implement our directional 4-port rectenna system, we focus on finding a hardwire configuration $\mathbf{x}$ to maximize the realized antenna gain of all ports over the frequency band of interest. This can be expressed as a binary optimization problem

$$\begin{aligned} \underset{\mathbf{x}}{\text{maximize}} \quad & \sum_{k=1}^{K}\sum_{i=1}^{4} G_{\mathrm{real}}^i(\mathbf{x}, f_k) \\ \text{subject to} \quad & \mathbf{x} \in \{0,1\}^Q \end{aligned} \tag{20}$$

where f_k denotes the kth (out of K) frequency samples in the frequency band of interest. Since our focus is the downlink channel of GSM-1800 (1.8-1.88 GHz) band, we maximize the sum of the realized antenna gain of all ports at 1.8, 1.82, ..., and 1.88 GHz.

The realized antenna gain $G_{\mathrm{real}}^i(\mathbf{x}, f_k)$ can be computed by electromagnetic solvers. In this work we compute them efficiently by a technique we refer to as *Internal Multi-Port Method* (IMPM) through the commercial solver CST Microwave Studio. IMPM is well suited for pixel antenna optimization as it can reduce the computational complexity significantly by using the techniques described in [48]-[50]. We also use the 90-degree rotational symmetry of the design to reduce computation time significantly.

A variety of optimization methods can be utilized but in this paper, we adopt *Successive Exhaustive Boolean Optimization* (SEBO) [51], which is shown to be efficient for pixel antenna optimization problems such as (20). The block size in SEBO is set $J = 8$ to solve the binary optimization problem (20).

The 4-port microstrip pixel patch antenna with the optimal hardwire configuration found by SEBO has been prototyped as shown in Fig. 6. The measured reflection coefficients and mutual couplings are shown in Fig. 7. The measured reflection coefficients S_{11}, S_{22}, S_{33}, and S_{44} are almost the same resulting from the 90-degree rotational symmetric hardwire configuration. The measured reflection coefficients and mutual couplings are all below -10 dB from 1.8 to 1.88 GHz, showing good impedance matching and isolation. The loaded-circuit radiation patterns (when measuring one port, the other ports are connected to 50 Ω) of the four ports are also measured by the SATIMO StarLab system. The measured loaded-circuit radiation patterns of the fours ports at 1.8 GHz on the XOZ plane and YOZ plane are shown in Fig. 8. The patterns of ports 1-4 are all uni-directional providing high directivity. We also find that the patterns of port 1 and port 4 are symmetric and also the patterns of port 2 and port 3 are symmetric, which results from the 90-degree rotational symmetry of the hardwire configuration. In addition, the patterns of ports 1-4 are slightly

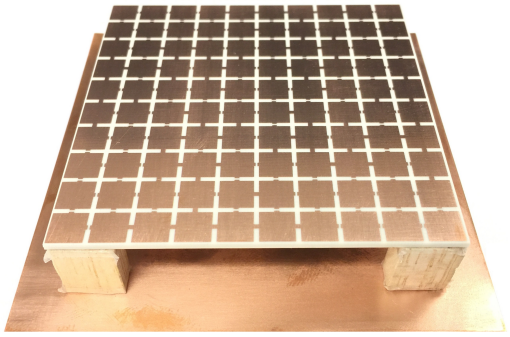

Fig. 6. Prototype of the 4-port microstrip pixel patch antenna with the optimal hardwire configuration.

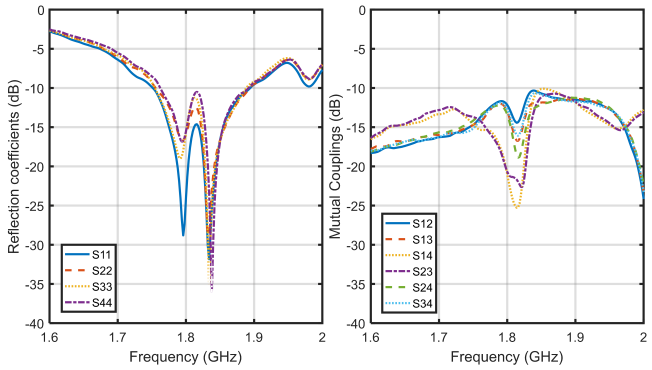

Fig. 7. Measured reflection coefficients and mutual couplings of the 4-port microstrip pixel patch antenna with the optimal hardwire configuration.

tilted from the broadside direction, which implies that angular diversity has been leveraged in the multiport antenna design to reduce mutual coupling. We can also find that the polarizations of port 1 and port 4 are orthogonal to the polarizations of port 2 and port 3, showing that our proposed multiport antenna is dual-polarized. Therefore, there is an advantage due to polarization diversity in our proposed multiport antenna, i.e. the randomly polarized ambient RF energy can be harvested to increase the average output dc power. The measured realized gains of ports 1-4 at 1.8 GHz are 5.52, 5.24, 5.37, and 5.75 dBi, respectively, and the total radiation efficiencies of ports 1-4 at 1.8 GHz are 66.0%, 63.5%, 64.9%, and 68.5%, respectively. The size of the 4-port microstrip pixel patch antenna is $0.6\times0.6\times0.1\lambda^3$. Each antenna port has a size of $0.3\times0.3\times0.1\lambda^3$ and realized antenna gain around 5.5 dBi. Therefore, the proposed 4-port microstrip pixel patch antenna implements the design of the compact multiport antenna with good realized antenna gain overall and should be close to the optimum possible for these design constraints.

B. Rectifier Design

We design and prototype a compact single series diode rectifier in GSM-1800 frequency band with size of $39 \times 19\,\mathrm{mm}^2$. The geometry and photo of the proposed rectifier is shown in Fig. 9. It consists of a matching network, a Schottky diode Avago HSMS-2850, a 1 nF capacitor, and a load resistor. The Schottky diode Skyworks SMS7630 is also a good choice for the rectifying diode due to its low turn-on

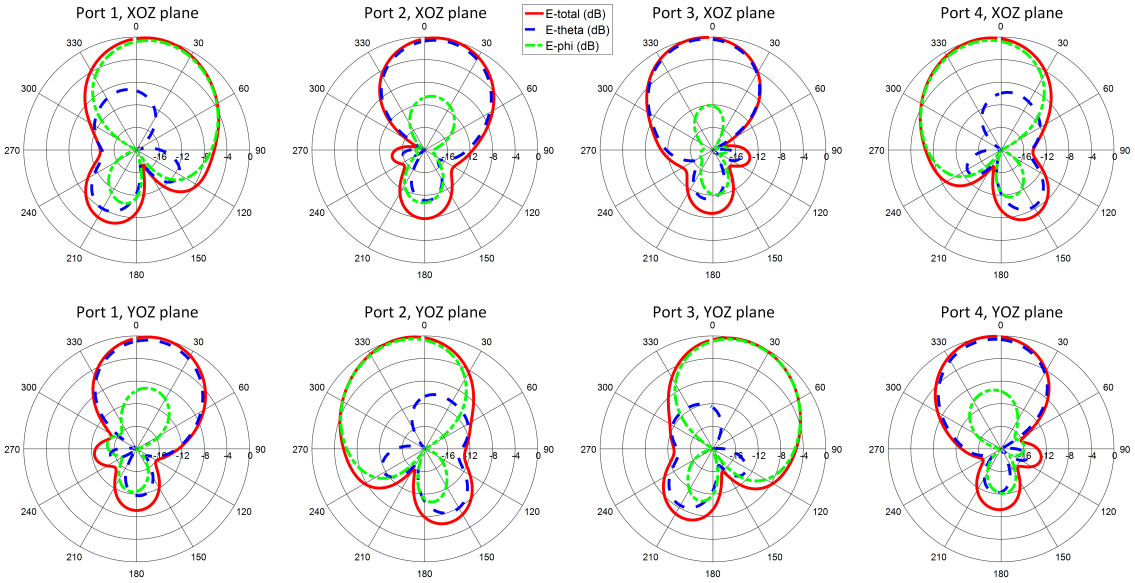

Fig. 8. Measured loaded-circuit radiation patterns of the 4-port microstrip pixel patch antenna with the optimal hardwire configuration.

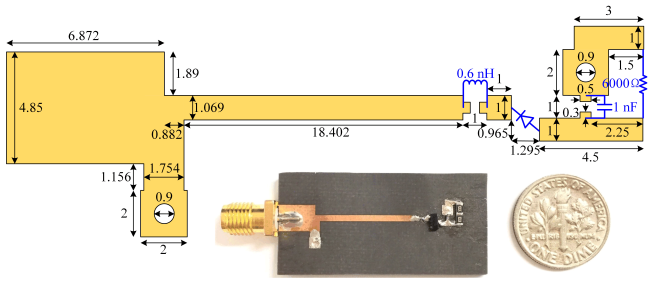

Fig. 9. Geometry and prototype of the single series diode rectifier (unit: mm).

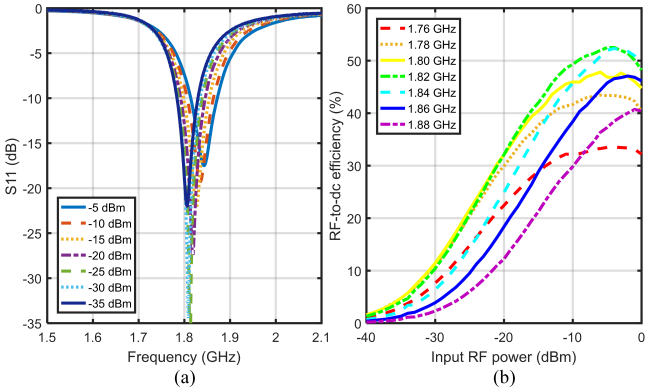

Fig. 10. (a) Measured reflection coefficient at different input power levels and (b) measured RF-to-dc efficiency at different frequencies of the single series diode rectifier.

voltage. It is fabricated on 62-mil-thick substrate RT/Duroid 5880 (dielectric constant $\epsilon_r = 2.2$) with low loss tangent of 0.0009 to reduce the insertion loss.

We adopt the single series diode rectifier topology because it maximizes the RF-to-dc efficiency at low input RF power compared with other topologies such as the voltage doubler rectifier [20] and Greinacher rectifier [21], as shown by a thorough study of rectifier topology in [52]. In ambient RF energy harvesting, rectifiers should operate at low input RF power because the power density of the ambient RF energy is very low. For a rectifier operating at low input RF power, there is a tradeoff between the RF-to-dc efficiency and the output dc voltage level. Increasing the number of diodes in the topology can increase the output dc voltage level, but it will decrease the RF-to-dc efficiency since more diodes cause additional loss. Therefore, the single series diode rectifier has been used in ambient RF energy harvesting due to its high RF-to-dc efficiency [7], [10], [13], [14], and we also use the single series diode rectifier to maximize the RF-to-dc efficiency and the output dc power. In addition, a power management unit (PMU) including dc-dc converter can be used to store the dc energy from the rectifier output and boost the dc voltage to provide a stable dc voltage supply for loads [7].

We simulate the rectifier by using the harmonic-balance (HB) solver in ADS with the nonlinear SPICE model of the Schottky diode Avago HSMS-2850. Because the performance of the rectifier is mainly determined by the load resistor for a given input RF power level, we optimize the load resistor in ADS to maximize the RF-to-dc efficiency at an input RF power of -20 dBm in the GSM-1800 frequency band. The optimized load resistor for -20 dBm input power is a $R_L = 6$ kΩ. For the matching network, we use single-stub tuning with a surface-mounted device (SMD) component, a 0.6 nH inductor from Murata, to implement impedance matching. The stub is grounded by a via to provide a dc circuit in the rectifier.

The measured reflection coefficients S_{11} of the proposed rectifier at different input power levels are shown in Fig. 10(a). Although the resonant frequency of the proposed rectifier slightly increases with the input RF power level due to the nonlinearity of the rectifier, the measured S_{11} shows that the proposed rectifier has good impedance matching for harvesting ambient RF energy in the GSM-1800 frequency band. We also

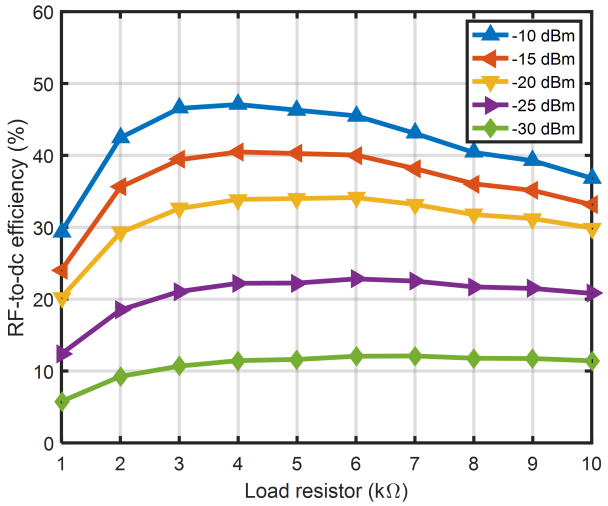

Fig. 11. Measured RF-to-dc efficiency of the single series diode rectifier versus load resistor at different input RF power levels and at 1.8 GHz.

evaluate the RF-to-dc efficiency of the proposed rectifier by connecting it to a signal generator and using a multimeter to measure the output dc voltage across the load resistor. The RF-to-dc efficiency of the rectifier is then obtained from $\eta = V_L^2/R_L P_{\text{in}}$ where V_L denotes the output dc voltage of the rectifier and P_{in} denotes the input RF power provided by the signal generator. The measured RF-to-dc efficiency of the proposed rectifier versus input RF power levels at different frequencies is shown in Fig. 10(b). We can find that the RF-to-dc efficiency increases with the input RF power until a turning point around -5 dBm, which shows the nonlinear behavior of the rectifier. The peak efficiencies over the GSM-1800 frequency band are 5.1% at -35 dBm, 11.9% at -30 dBm, 22.5% at -25 dBm, 33.4% at -20 dBm, 43.4% at -15 dBm, 51.3% at -10 dBm, and 55.1% at -5 dBm, showing good rectification efficiency at low input RF power levels. In addition, the rectifier can still work with an efficiency of 1.6% at the extremely low input RF power of -40 dBm. The measured RF-to-dc efficiency of the proposed rectifier versus load resistor at different input RF power levels and at 1.8 GHz is shown in Fig. 11. We can find that the measured RF-to-dc efficiency is maximum at 6 kΩ at low input RF power ranging from -30 dBm to -15 dBm. This is consistent with optimizing the load resistor in ADS simulation to maximize the efficiency. In addition, we can find that the measured RF-to-dc efficiency of our proposed rectifier at low input RF power does not decrease much when the load resistor deviates from the optimal value of 6 kΩ.

C. DC Combining Design

DC combining is used for the proposed directional 4-port rectenna system to add the output dc power of each rectifier to the load. We fabricate four rectifiers as shown in Fig. 9 and each rectifier is connected to an antenna port to rectify the RF power received by each antenna port. The efficiency of the dc combining circuit is important for increasing the average output dc power. To achieve high dc combining efficiency,

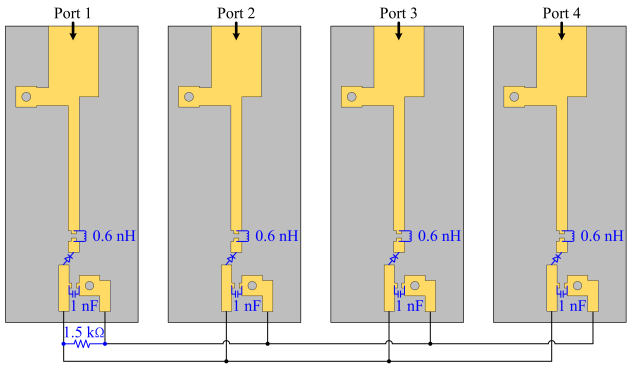

Fig. 12. Topology of the parallel dc combining circuit for the 4-port rectenna.

we can use a multiple-input multiple-output switching dc-dc converter to combine the output dc power of each rectifier [53]-[55]. However, considering the circuit complexity and high cost, in this work we use a straightforward parallel dc combining circuit. The topology of the parallel dc combining circuit for the 4-port rectenna is shown in Fig. 12. In Fig. 12, there are four rectifiers and each rectifier is connected to an antenna port. The dc outputs of the four rectifiers are connected in parallel to increase the output dc current. Accordingly, the corresponding load resistor is then decreased to $R_L = 1.5\,\text{k}\Omega$ since we have 4 ports [56]. In addition, for each rectifier, the capacitor at the output is 1 nF. It should be noted that connecting the dc outputs of the four rectifiers in series will short the diodes because the four antenna ports share the same ground. Therefore, series dc combining is not applicable for our proposed 4-port rectenna.

V. Directional Multiport Ambient RF Energy Harvesting System Measurement

To demonstrate the effectiveness of the proposed directional 4-port rectenna for average output dc power maximization, we compare it with a reference omni-directional single-port monopole rectenna and a reference directional single-port patch rectenna.

The omni-directional single-port monopole rectenna consists of a single-port monopole antenna as shown in Fig. 13(a) and a single series diode rectifier as shown in Fig. 9. The single-port monopole antenna is fabricated on Rogers 4003 substrate and fed by a microstrip line. It has a similar size to the proposed 4-port pixel patch antenna. We measure the S_{11} and radiation pattern of the single-port monopole antenna and it shows a good impedance matching and an omni-directional pattern at the GSM-1800 band. The measured realized gain and total radiation efficiency of the single-port monopole antenna at 1.8 GHz is 1.62 dBi and 80%, respectively. On the other hand, the directional single-port patch rectenna consists of a single-port patch antenna as shown in Fig. 13(b) and a single series diode rectifier as shown in Fig. 9. The single-port patch antenna is fed by L-probe and the microstrip line and the patch are printed on the Rogers 4003 substrate. It also has the same size to the proposed 4-port pixel patch antenna. We measure the S_{11} and radiation pattern of the single-port

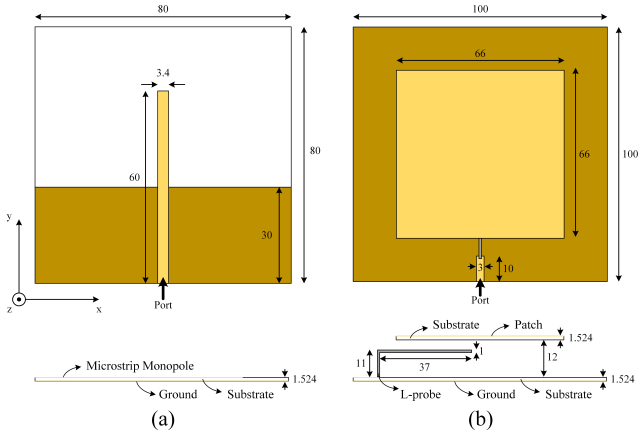

Fig. 13. Plan view and elevation view of (a) the single-port monopole antenna and (b) the single-port patch antenna (unit: mm).

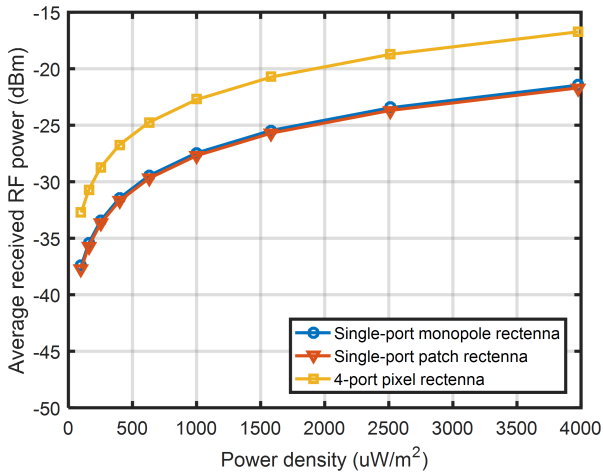

Fig. 14. Average received RF power of the single-port monopole rectenna, the single-port patch rectenna, and the 4-port pixel patch rectenna versus the power density at 1.8 GHz.

patch antenna and it shows a good impedance matching and an uni-directional pattern at the GSM-1800 band. The measured realized gain and total radiation efficiency of the single-port patch antenna at 1.8 GHz is 7.6 dBi and 80%, respectively. We find that the single-port monopole and patch antenna have low and high antenna directivity, respectively. Therefore, we select them as benchmarks to demonstrate the effect of antenna directivity on the average received RF and average output dc power and also to show the advantages of the proposed directional 4-port rectenna.

The experimental setup corresponds to an approximation to RF energy harvesting in an ambient RF environment. For the average received RF power, we measure it in three steps: 1) we measure the radiation patterns of the proposed antenna and the two benchmark antennas; 2) we assume a random RF field with a 3-D uniform PAS; 3) we estimate the average received RF power using the measured radiation patterns and assumed random RF field. On the other hand, for the average output dc power, we measure it in four steps: 1) we replace antenna ports with signal generators; 2) we set the RF power levels of signal generators according to the RF power received by antenna ports; 3) we connect the signal generators to the rectifier prototypes; 4) we measure the output dc power of the rectifier prototypes using multi-meter. We use this setup because it is difficult to build an experimental setup to generate the random RF field with 3-D uniform PAS in reality. In addition, the load resistor for the single-port monopole rectenna, the single-port patch rectenna, and the proposed 4-port rectenna are 6 kΩ, 6 kΩ, and 1.5 kΩ, respectively.

A. Average Received RF Power

First, we compare the average received RF power of the single-port monopole rectenna, the single-port patch rectenna, and the proposed 4-port pixel patch rectenna. The average received RF power of the three rectenna versus the power density at 1.8 GHz is shown in Fig. 14.

We make the following observations from Fig. 14. *Firstly*, we find that the single-port monopole rectenna and the single-port patch rectenna have the same average received RF power, which verifies that the antenna directivity does not affect the average received RF power. *Secondly*, we find that the proposed 4-port pixel patch rectenna has 4.73 dB more average received RF power than the single-port monopole and patch rectenna. The improvement in the average received RF power is because the proposed rectenna has more antenna ports and the improvement is constant no matter how the power density changes. From Section II.B, the increase of average received RF power should be 6 dB but due to the multiport antenna having less efficiency than the single-port antenna so that the increase is only 4.7 dB.

Overall, the two observations made from Fig. 14 show that the measurement results match well with the theoretical analysis (7)-(10) in terms of the average received RF power.

B. Average Output DC Power

Next, we compare the average output dc power of the three rectennas. For simplicity, we replace antenna ports with signal generators and connect the signal generator to the rectifier prototype input to simulate the RF power received by each antenna port at different incident angles and at different power densities above. The RF power levels of the signal generators are set according to the received RF power found by the loaded-circuit radiation patterns and assumed power densities. Because the antennas have good impedance matching and the RF power level is based on the measured radiation pattern, the approximation by replacing the antenna ports with signal generators is accurate and reasonable. The output dc voltage is measured by a multimeter and is used to compute the output dc power. Averaging the output dc power over all the incident angles, we can therefore find the average output dc power of the three rectennas at different power densities and this provided at 1.8 GHz in Fig. 15. We also find the average output dc power of the 4-port pixel patch rectenna with perfect dc combining and plot it in Fig. 15.

We make the following observations from Fig. 15. *Firstly*, comparing the two reference rectennas, we find that the single-port patch rectenna can provide more average output dc power

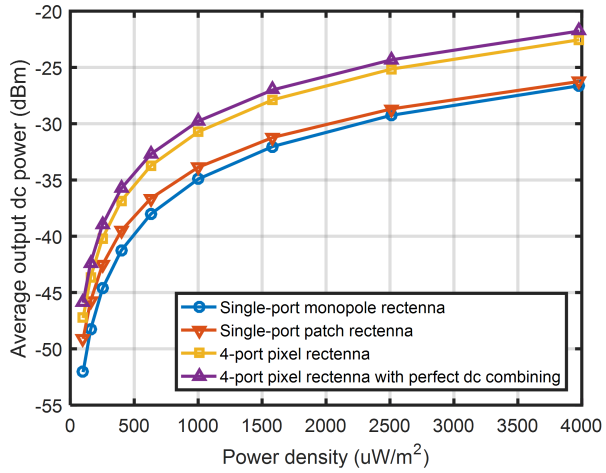

Fig. 15. Average output dc power of the single-port monopole rectenna, the single-port patch rectenna, and the 4-port pixel patch rectenna versus the power density at 1.8 GHz.

than the single-port monopole rectenna. At a power density of 100 $\mu\mathrm{W/m^2}$, the improvement is 2.9 dB, however at 4000 $\mu\mathrm{W/m^2}$ the improvement is only 0.4 dB. The improvement of the average output dc power is because the single-port patch rectenna has higher antenna directivity than the single-port monopole rectenna, demonstrating the effect of antenna directivity on the average output dc power. In addition, it is demonstrated that such effect becomes weak at high power density, which is due to the nonlinear RF-to-dc efficiency verses input power characteristic of the rectifier as shown in Fig. 10(b). This is consistent with the numerical simulation results shown in Fig. 4.

Secondly, compared with the reference single-port patch rectenna, the proposed 4-port pixel patch rectenna provides more average output dc power. When the power density increases from 100 to 4000 $\mu\mathrm{W/m^2}$, the average output dc power difference between the 4-port pixel patch rectenna with perfect dc combining and the single-port patch rectenna increases from 3.2 to 4.5 dB while the difference between the 4-port pixel patch rectenna with the parallel dc combining and the single-port patch rectenna increases from 1.9 to 3.7 dB. The improvement is because the 4-port pixel patch rectenna has more antenna ports, demonstrating that the average output dc power increases linearly with the number of antenna ports. We also find that the improvement is weak at low power density because the single-port patch rectenna has higher antenna directivity than the 4-port pixel patch rectenna.

Thirdly, compared with the reference single-port monopole rectenna, the 4-port pixel patch rectenna provide more average output dc power (up to 6.2 dB) than the single-port monopole rectenna. When the power density increases from 100 to 4000 $\mu\mathrm{W/m^2}$, the average output dc power difference between the 4-port pixel patch rectenna with perfect dc combining and the single-port monopole rectenna decreases from 6.2 to 4.9 dB while the difference between the 4-port pixel patch rectenna with the parallel dc combining and the single-port monopole rectenna decreases from 4.8 to 4.1 dB. This improvement is not only because the 4-port pixel patch rectenna has more antenna ports but also has higher antenna directivity. In addition, we can find that this improvement is weak at high power density because the 4-port pixel patch rectenna has higher antenna directivity than the single-port monopole rectenna. This again demonstrates that high antenna directivity can boost the average output dc power but the advantage decreases when the power density increases.

Lastly, the difference between the average output dc power of the 4-port pixel patch rectenna with perfect dc combining and with parallel dc combining is around 1 dB, which implies that the efficiency of the parallel dc combining circuit is around 80%. The reason why the parallel dc combining circuit cannot have 100% efficiency is because the input RF power to each rectifier is different due to the different radiation pattern of each antenna port. In the dc circuit of the four rectifiers with parallel dc combining, four diodes are in shunt with a load resistor so that the working condition of each port will influence the other three ports. When the input RF power to each rectifier is different, each rectifier will deviate from its optimal working condition so the overall rectifying performance will be degraded. To solve this problem, we can use a multiple-input multiple-output switching dc-dc converter to match all the rectifiers to their optimum working condition [54], [55]. Therefore nearly perfect dc combining efficiency can be achieved. Overall, in spite of the the dc combining efficiency degradation, the parallel dc combining circuit has good performance with simple circuit structure and low cost.

To conclude, the proposed directional 4-port pixel patch rectenna can increase the average output dc power by up to 4.5 dB compared with the single-port patch rectenna and by up to 6.2 dB compared with the single-port monopole rectenna. The observations made from Fig. 15 show that the measurement results match well with the theoretical analysis (19) that the average output dc power increases linearly with the number of antenna ports and increases nonlinearly with the antenna directivity.

C. Measurement in Real Ambient Environment

To further demonstrate the benefit of the proposed rectenna design, we measure the proposed rectenna and the two benchmark rectennas in a real ambient environment outdoors at the Hong Kong University of Science and Technology as shown in Fig. 16. For the single-port monopole rectenna, the measured output dc voltage is around 80 mV and can reach 92.8 mV as shown in Fig. 16(a), which corresponds to an output dc power of 1.4 μW (the load is 6 kΩ). For the single-port patch rectenna, the measured output dc voltage is around 100 mV and can reach 112.7 mV as shown in Fig. 16(b), which corresponds to an output dc power of 2.1 μW (the load is 6 kΩ) higher than that of the single-port monopole rectenna. This demonstrates the benefit of increasing antenna directivity to increase the dc power. On the other hand, for the proposed 4-port pixel patch rectenna, the measured output dc voltage is around 110 mV and can reach to 129.9 mV as shown in Fig. 16(c), which corresponds to an output dc power of 11.2 μW (the load is 1.5 kΩ with the parallel dc combining). Therefore, using the proposed rectenna can achieve five times

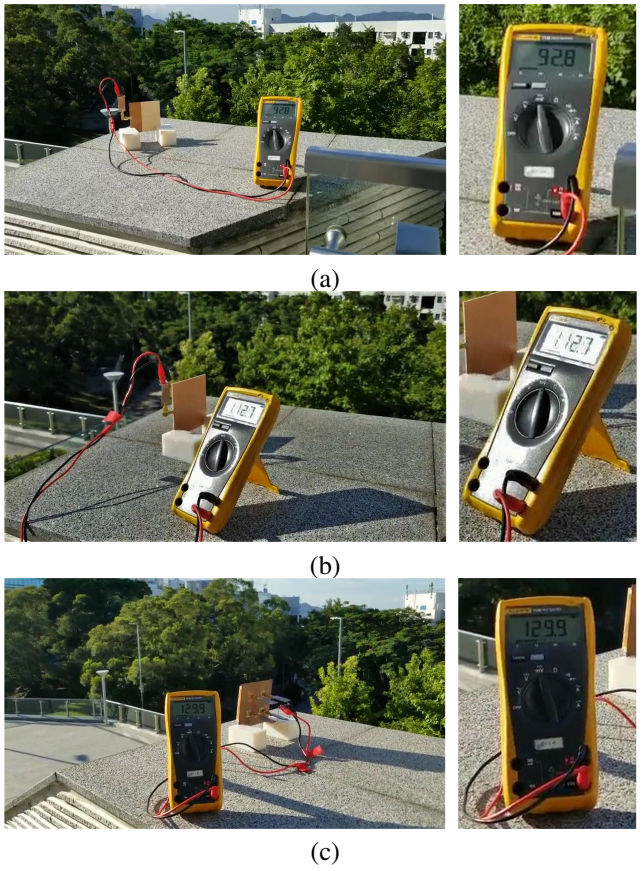

Fig. 16. Photos of the measurement in a real ambient environment with (a) the single-port monopole rectenna, (b) the single-port patch rectenna, and (c) the 4-port pixel patch rectenna (units on the display are in mV).

higher output dc power than the two conventional benchmark rectennas in reality. Our proposed rectenna performs better because of both the multiple antenna ports and also the good antenna gain, as analyzed by the theoretical model in Section II. Hence, using directional multiport rectenna is beneficial to overcome the challenge of low power density in ambient RF environment.

We also provide a comparison of the proposed rectenna with related work in Table I. We can find that our proposed rectenna implements multiple antenna ports with high realized gain in a compact size. Compared with other rectennas, our proposed rectenna has more ports and smaller average antenna size for each port while having higher realized gain, showing a good directional multiport rectenna design. Particularly, we define a figure of merit (FoM) as

$$\text{FoM} = \frac{\sum_{n=1}^{N} A_n}{A_{\text{phy}}} = \frac{\lambda^2}{4\pi A_{\text{phy}}} \sum_{n=1}^{N} G_{\text{real}}^n \tag{21}$$

where A_{phy} refers to the physical aperture of the N-port antenna, A_n refers to the antenna effective aperture of the nth port, and G_{real}^n refers to the realized gain of the nth port. According to the definition of FoM (21), large FoM implies more antenna ports and/or higher antenna gain given a fixed antenna area, which is beneficial to increase the average output dc power as shown in Section II. Therefore, we include the FoM in Table I and we can find that our proposed rectenna has the highest FoM, again showing the good performance of our directional multiport rectenna design. Furthermore, we can stack two 4-port pixel patch antennas back to back as proposed in [17] to double the number of antenna ports without affecting the antenna area and gain, so that the FoM can be further doubled. Besides, our rectifier has good RF-to-dc efficiency at the low input RF power. Therefore, the proposed 4-port pixel patch rectenna is well suited for ambient RF energy harvesting.

VI. Conclusion

We have shown that for ambient RF energy harvesting the average *output dc power* increases nonlinearly with antenna directivity and increases linearly with the number of antenna ports through analysis and numerical simulation. Therefore to maximize average output dc power the number of antenna ports should be maximized as well as the antenna directivity. However, the increase in harvested energy through adding additional antennas in a fixed area or volume does not come without physical limits such as mutual coupling. Besides, increasing directivity increases antenna size. So the design challenge is to fit as many compact antennas into the fixed area or volume with the lowest mutual coupling acceptable for RF energy harvesting with highest directivity possible. Meeting this challenge opens up the possibility of utilizing ambient RF energy harvesting for IoT applications.

Motivated by these findings and challenges, we have developed an optimized directional multiport rectenna system to maximize the average output dc power. It operates at GSM-1800 frequency band and consists of a 4-port microstrip pixel patch antenna, four single series diode rectifiers, and parallel dc combining. The 4-port microstrip pixel patch antenna has an average antenna size for each port of $0.3\lambda \times 0.3\lambda$ and realized gains of 5.5 dBi for each port. The single series diode rectifier shows good impedance matching and high RF-to-dc efficiency of 11.9% at -30 dBm, 33.4% at -20 dBm, and 51.3% at -10 dBm.

We compare the proposed 4-port pixel patch rectenna with two reference rectennas, a single-port monopole rectenna and a single-port patch rectenna. Measurement results show that the proposed 4-port pixel patch rectenna increases average output dc power by up to 4.5 dB compared with the single-port patch rectenna and by up to 6.2 dB compared with the single-port monopole rectenna. It also shows that the parallel dc combining circuit has an efficiency of around 80%. We also measure the proposed rectenna and the two reference rectennas in a real ambient environment. Measurement results show that the proposed rectenna can achieve an output dc power of 11.2 μW which is five times higher than that of the two reference rectennas.

Future work could include the extension to multi-band/broadband and multi-polarized directional multiport rectennas to further increase the output dc power for ambient RF energy harvesting.

Acknowledgment

We wish to gratefully acknowledge Prof. Charles G. Sodini for his support. We also wish to gratefully acknowledge

TABLE I
COMPARISON OF THE PROPOSED RECTENNA AND RELATED WORK

Ref.	Frequency (GHz)*	Average antenna size of each port in λ**	Port No.	Realized gain	FoM#	Rectifier RF-to-dc efficiency performance
[14]	Dual-band 0.915, 2.45	0.18×0.18×0.18†	1	1.87 dBi@0.915 GHz 4.18 dBi@2.45 GHz	N.A.	13%@-20 dBm, 0.915 GHz 10%@-20 dBm, 2.45 GHz
[15]	Dual-band 0.915, 2.45	N.A.	1	N.A.	N.A.	23%@-15 dBm, 0.915 GHz 21%@-15 dBm, 2.5 GHz
[17]	Triple-band 0.94, 1.84, 2.14	0.39×0.44	2	8.15 dBi@0.94 GHz, Port 1, 2 7.15 dBi@1.84 GHz, Port 1, 2 8.15 dBi@2.14 GHz, Port 1, 2	3.03	27.3%@-20 dBm, 0.94 GHz 20%@-20 dBm, 1.84 GHz 14%@-20 dBm, 2.14 GHz
[18]	Triple-band 2, 2.5, 3.5	0.8×0.8	1	7 dBi@2 GHz 5.5 dBi@2.5 GHz 9.2 dBi@3.5 GHz	0.62	20% @2 GHz 7% @2.5 GHz 5% @3.5 GHz
[19]	Quad-band 0.9, 1.8, 2.1, 2.4	0.3×0.3††	1	6 dBi from 0.9 to 3 GHz	N.A.	16%@-20 dBm, 0.9 GHz 15%@-20 dBm, 1.8 GHz 14%@-20 dBm, 2.1 GHz 14%@-20 dBm, 2.4 GHz
[20]	Hexa-band 0.55, 0.75, 0.9, 1.85, 2.15, 2.45	0.3×0.3	1	2.5 dBi@0.55 GHz 3.1 dBi@0.75 GHz 3.6 dBi@0.9 GHz 5 dBi@1.85 GHz 5 dBi@2.15 GHz 4.5 dBi@2.45 GHz	1.57	25%@-20 dBm, 0.55 GHz 20%@-20 dBm, 0.75 GHz 25%@-20 dBm, 0.9 GHz 15%@-20 dBm, 1.85 GHz 9%@-20 dBm, 2.15 GHz 5%@-20 dBm, 2.45 GHz
[21]	Broad-band 1.8, 2.5	0.42×0.42	1	2.5 dBi@1.8 GHz 4 dBi@2.5 GHz	0.80	33%@-20 dBm, 1.8 GHz 13%@-20 dBm, 2.5 GHz
[22]	Broad-band 0.98, 1.8	0.27×0.23	1	higher than 2 dBi from 0.98 to 1.8 GHz	2.03	35.2%@4.7 dBm, 0.98 GHz 6%@5.4 dBm, 1.8 GHz
[24]	Single-band 2.45	0.57×0.56	6	5 dBi@2.45 GHz, Ports 1-6	0.79	35%@-10 dBm, 2.45 GHz 15%@-20 dBm, 2.45 GHz
[28]	Single-band 1.84	0.42×0.42	4	3.3 dBi@1.84 GHz, Ports 1-4	0.96	35%@-10 dBm, 1.84 GHz 21.5%@-20 dBm, 1.84 GHz 5.1%@-30 dBm, 1.84 GHz
[29]	Single-band 1.84	0.2×0.34	3	3.83 dBi@1.84 GHz, Port 1 2.36 dBi@1.84 GHz, Port 2 3.90 dBi@1.84 GHz, Port 3	2.57	31.5%@-10 dBm, 1.84 GHz 21.1%@-20 dBm, 1.84 GHz 6.9%@-30 dBm, 1.84 GHz
This work	Single-band 1.8	0.3×0.3	4	5.52 dBi@1.8 GHz, Port 1 5.24 dBi@1.8 GHz, Port 2 5.37 dBi@1.8 GHz, Port 3 5.75 dBi@1.8 GHz, Port 4	3.12	51.3%@-10 dBm, 1.8 GHz 33.4%@-20 dBm, 1.8 GHz 11.9%@-30 dBm, 1.8 GHz

* Central frequency of each band for multi-band rectenna, while lowest and highest operating frequency for broad-band rectenna.
** λ is the wavelength referring to the lowest frequency of antenna operation.
† The antenna is not a planar antenna, so it is not applicable to find the FoM.
†† The antenna size does not include the reflector plane, so it is not applicable to find the FoM.
# For multi-band/broad-band antenna, we only consider the FoM at its lowest frequency of antenna operation.

the funding support for this research from grant 16207314 provided by the Hong Kong Research Grants Council.

REFERENCES

[1] S. Kim, R. Vyas, J. Bito, K. Niotaki, A. Collado, A. Georgiadis, and M. M. Tentzeris, "Ambient RF energy-harvesting technologies for self-sustainable standalone wireless sensor platforms," *Proceedings of the IEEE*, vol. 102, no. 11, pp. 1649–1666, Nov. 2014.

[2] A. Omairi, Z. H. Ismail, K. A. Danapalasingam, and M. Ibrahim, "Power harvesting in wireless sensor networks and its adaptation with maximum power point tracking: Current technology and future directions," *IEEE Internet Things J.*, vol. 4, no. 6, pp. 2104–2115, 2017.

[3] O. B. Akan, O. Cetinkaya, C. Koca, and M. Ozger, "Internet of hybrid energy harvesting things," *IEEE Internet Things J.*, vol. 5, no. 2, pp. 736–746, 2018.

[4] X. Yue, M. Kauer, M. Bellanger, O. Beard, M. Brownlow, D. Gibson, C. Clark, C. MacGregor, and S. Song, "Development of an indoor photovoltaic energy harvesting module for autonomous sensors in building air quality applications," *IEEE Internet Things J.*, vol. 4, no. 6, pp. 2092–2103, 2017.

[5] P. Chen, T. Su, and P. M. Fan, "Thermoelectric energy harvesting interface circuit with capacitive bootstrapping technique for energy-efficient IoT devices," *IEEE Internet Things J.*, vol. 5, no. 5, pp. 4058–4065, 2018.

[6] F. Deng, X. Yue, X. Fan, S. Guan, Y. Xu, and J. Chen, "Multisource energy harvesting system for a wireless sensor network node in the field environment," *IEEE Internet Things J.*, vol. 6, no. 1, pp. 918–927, 2019.

[7] M. Piñuela, P. D. Mitcheson, and S. Lucyszyn, "Ambient RF energy harvesting in urban and semi-urban environments," *IEEE Trans. Microw. Theory Techn.*, vol. 61, no. 7, pp. 2715–2726, Jul. 2013.

[8] U. Muncuk, K. Alemdar, J. D. Sarode, and K. R. Chowdhury, "Multi-band ambient RF energy harvesting circuit design for enabling battery-less sensors and IoT," *IEEE Internet Things J.*, vol. 5, no. 4, pp. 2700–2714, 2018.

[9] Y. Shi, Y. Fan, Y. Li, L. Yang, and M. Wang, "An efficient broadband slotted rectenna for wireless power transfer at LTE band," *IEEE Trans. Antennas Propag.*, vol. 67, no. 2, pp. 814–822, Feb 2019.

[10] X. Wang and A. Mortazawi, "Medium wave energy scavenging for wireless structural health monitoring sensors," *IEEE Trans. Microw. Theory Techn.*, vol. 62, no. 4, pp. 1067–1073, Apr. 2014.

[11] R. J. Vyas, B. B. Cook, Y. Kawahara, and M. M. Tentzeris, "E-WEHP: A batteryless embedded sensor-platform wirelessly powered from ambient digital-TV signals," *IEEE Trans. Microw. Theory Techn.*, vol. 61, no. 6, pp. 2491–2505, Jun. 2013.

[12] H. Sun, Y.-X. Guo, M. He, and Z. Zhong, "Design of a high-efficiency 2.45-GHz rectenna for low-input-power energy harvesting," *IEEE Antennas Wireless Propag. Lett.*, vol. 11, pp. 929–932, 2012.

[13] ——, "A dual-band rectenna using broadband yagi antenna array for ambient RF power harvesting," *IEEE Antennas Wireless Propag. Lett.*, vol. 12, pp. 918–921, 2013.

[14] K. Niotaki, S. Kim, S. Jeong, A. Collado, A. Georgiadis, and M. M.

Tentzeris, "A compact dual-band rectenna using slot-loaded dual band folded dipole antenna," *IEEE Antennas Wireless Propag. Lett.*, vol. 12, pp. 1634–1637, 2013.

[15] K. Niotaki, A. Georgiadis, A. Collado, and J. S. Vardakas, "Dual-band resistance compression networks for improved rectifier performance," *IEEE Trans. Microw. Theory Techn.*, vol. 62, no. 12, pp. 3512–3521, Dec. 2014.

[16] S. Shen, C.-Y. Chiu, and R. D. Murch, "A broadband L-probe microstrip patch rectenna for ambient RF energy harvesting," in *Proc. IEEE Int. Symp. Antennas Propag. USNC/URSI Nat. Radio Sci. Meeting*, 2017, pp. 2037–2038.

[17] S. Shen, C. Y. Chiu, and R. D. Murch, "A dual-port triple-band L-probe microstrip patch rectenna for ambient RF energy harvesting," *IEEE Antennas Wireless Propag. Lett.*, vol. 16, pp. 3071–3074, 2017.

[18] S. Chandravanshi, S. S. Sarma, and M. J. Akhtar, "Design of triple band differential rectenna for RF energy harvesting," *IEEE Trans. Antennas Propag.*, vol. 66, no. 6, pp. 2716–2726, June 2018.

[19] V. Kuhn, C. Lahuec, F. Seguin, and C. Person, "A multi-band stacked RF energy harvester with RF-to-DC efficiency up to 84%," *IEEE Trans. Microw. Theory Techn.*, vol. 63, no. 5, pp. 1768–1778, May 2015.

[20] C. Song *et al.*, "A novel six-band dual CP rectenna using improved impedance matching technique for ambient RF energy harvesting," *IEEE Trans. Antennas Propag.*, vol. 64, no. 7, pp. 3160–3171, July 2016.

[21] C. Song, Y. Huang, J. Zhou, J. Zhang, S. Yuan, and P. Carter, "A high-efficiency broadband rectenna for ambient wireless energy harvesting," *IEEE Trans. Antennas Propag.*, vol. 63, no. 8, pp. 3486–3495, Aug. 2015.

[22] M. Arrawatia, M. S. Baghini, and G. Kumar, "Broadband bent triangular omnidirectional antenna for RF energy harvesting," *IEEE Antennas Wireless Propag. Lett.*, vol. 15, pp. 36–39, 2016.

[23] J. A. Hagerty, F. B. Helmbrecht, W. H. McCalpin, R. Zane, and Z. B. Popovic, "Recycling ambient microwave energy with broad-band rectenna arrays," *IEEE Trans. Microw. Theory Techn.*, vol. 52, no. 3, pp. 1014–1024, Mar. 2004.

[24] D. Vital, S. Bhardwaj, and J. L. Volakis, "Textile-based large area RF-power harvesting system for wearable applications," *IEEE Trans. Antennas Propag.*, vol. 68, no. 3, pp. 2323–2331, 2020.

[25] T. S. Almoneef, H. Sun, and O. M. Ramahi, "A 3-D folded dipole antenna array for far-field electromagnetic energy transfer," *IEEE Antennas Wireless Propag. Lett.*, vol. 15, pp. 1406–1409, 2016.

[26] B. K. Lau, J. B. Andersen, G. Kristensson, and A. F. Molisch, "Impact of matching network on bandwidth of compact antenna arrays," *IEEE Trans. Antennas Propag.*, vol. 54, no. 11, pp. 3225–3238, Nov. 2006.

[27] S. Shen and R. D. Murch, "Impedance matching for compact multiple antenna systems in random RF fields," *IEEE Trans. Antennas Propag.*, vol. 64, no. 2, pp. 820–825, Feb. 2016.

[28] S. Shen, Y. Zhang, C.-Y. Chiu, and R. D. Murch, "A compact quad-port dual-polarized dipole rectenna for ambient RF energy harvesting," in *2018 12th European Conference on Antennas and Propagation*, London, United Kingdom, Apr. 2018.

[29] S. Shen, C. Y. Chiu, and R. D. Murch, "Multiport pixel rectenna for ambient RF energy harvesting," *IEEE Trans. Antennas Propag.*, vol. 66, no. 2, pp. 644–656, Feb. 2018.

[30] S. Shen and R. D. Murch, "Designing dual-port pixel antenna for ambient RF energy harvesting using genetic algorithm," in *Proc. IEEE Int. Symp. Antennas Propag. (APSURSI)*, July 2015, pp. 1286–1287.

[31] A. Georgiadis, G. V. Andia, and A. Collado, "Rectenna design and optimization using reciprocity theory and harmonic balance analysis for electromagnetic (EM) energy harvesting," *IEEE Antennas Wireless Propag. Lett.*, vol. 9, pp. 444–446, 2010.

[32] H. Sun and W. Geyi, "A new rectenna with all-polarization-Receiving capability for wireless power transmission," *IEEE Antennas Wireless Propag. Lett.*, vol. 15, pp. 814–817, 2016.

[33] J.-H. Chou, D.-B. Lin, K.-L. Weng, and H.-J. Li, "All polarization receiving rectenna with harmonic rejection property for wireless power transmission," *IEEE Trans. Antennas Propag.*, vol. 62, no. 10, pp. 5242–5249, Oct. 2014.

[34] S. Shen, Y. Zhang, C.-Y. Chiu, and R. D. Murch, "An ambient RF energy harvesting system where the number of antenna ports is dependent on frequency," *IEEE Trans. Microw. Theory Tech.*, vol. 67, no. 9, pp. 3821–3832, Sep. 2019.

[35] E. Vandelle *et al.*, "Harvesting ambient RF energy efficiently with optimal angular coverage," *IEEE Trans. Antennas Propag.*, vol. 67, no. 3, pp. 1862–1873, March 2019.

[36] Y.-Y. Hu, S. Sun, H. Xu, and H. Sun, "Grid-array rectenna with wide angle coverage for effectively harvesting RF energy of low power density," *IEEE Trans. Microw. Theory Techn.*, vol. 67, no. 1, pp. 402–413, Jan 2019.

[37] U. Olgun, C.-C. Chen, and J. L. Volakis, "Investigation of rectenna array configurations for enhanced RF power harvesting," *IEEE Antennas Wireless Propag. Lett.*, vol. 10, pp. 262–265, 2011.

[38] D. Lee *et al.*, "Hybrid power combining rectenna array for wide incident angle coverage in RF energy transfer," *IEEE Trans. Microw. Theory Techn.*, vol. 65, no. 9, pp. 3409–3418, Sep. 2017.

[39] S. Shen *et al.*, "A triple-band high-gain multibeam ambient RF energy harvesting system utilizing hybrid combining," *IEEE Trans. Ind. Electron.*, accepted, 2019.

[40] Z. Zeng *et al.*, "Design of sub-gigahertz reconfigurable RF energy harvester from -22 to 4 dBm with 99.8% peak MPPT power efficiency," *IEEE J. Solid-State Circuits*, vol. 54, no. 9, pp. 2601–2613, Sep. 2019.

[41] Y. Zhang *et al.*, "Hybrid RF-solar energy harvesting systems utilizing transparent multiport micromeshed antennas," *IEEE Trans. Microw. Theory Tech.*, vol. 67, no. 11, pp. 4534–4546, Nov 2019.

[42] W. Lin, R. W. Ziolkowski, and J. Huang, "Electrically small, low profile, highly efficient, huygens dipole rectennas for wirelessly powering internet-of-Things (IoT) devices," *IEEE Trans. Antennas Propag.*, vol. 67, no. 6, pp. 3670–3679, June 2019.

[43] T. S. Almoneef, F. Erkmen, M. A. Alotaibi, and O. M. Ramahi, "A new approach to microwave rectennas using tightly coupled antennas," *IEEE Trans. Antennas Propag.*, vol. 66, no. 4, pp. 1714–1724, 2018.

[44] T. S. Almoneef, F. Erkmen, and O. M. Ramahi, "Harvesting the energy of multi-polarized electromagnetic waves," *Scientific reports*, vol. 7, no. 1, pp. 1–14, 2017.

[45] R. G. Vaughan and J. B. Andersen, "Antenna diversity in mobile communications," *IEEE Trans. Veh. Technol.*, vol. 36, no. 4, pp. 149–172, Nov. 1987.

[46] R. E. Collin, *Antennas and radiowave propagation*. McGraw-Hill New York, 1985, vol. 6.

[47] B. Clerckx, A. Costanzo, A. Georgiadis, and N. Borges Carvalho, "Toward 1G mobile power networks: RF, signal, and system designs to make smart objects autonomous," *IEEE Microw. Mag.*, vol. 19, no. 6, pp. 69–82, Sep. 2018.

[48] S. Song and R. D. Murch, "An efficient approach for optimizing frequency reconfigurable pixel antennas using genetic algorithms," *IEEE Trans. Antennas Propag.*, vol. 62, no. 2, pp. 609–620, Feb. 2014.

[49] P. Lotfi, S. Soltani, and R. D. Murch, "Printed endfire beam-steerable pixel antenna," *IEEE Trans. Antennas Propag.*, vol. 65, no. 8, pp. 3913–3923, Aug. 2017.

[50] J. Araque Quijano and G. Vecchi, "Optimization of an innovative type of compact frequency-reconfigurable antenna," *IEEE Trans. Antennas Propag.*, vol. 57, no. 1, pp. 9–18, Jan. 2009.

[51] S. Shen, Y. Sun, S. Song, D. P. Palomar, and R. D. Murch, "Successive boolean optimization of planar pixel antennas," *IEEE Trans. Antennas Propag.*, vol. 65, no. 2, pp. 920–925, Feb. 2017.

[52] Y. Chen and C. Chiu, "Maximum achievable power conversion efficiency obtained through an optimized rectenna structure for RF energy harvesting," *IEEE Trans. Antennas Propag.*, vol. 65, no. 5, pp. 2305–2317, 2017.

[53] Y. H. Lam, W. H. Ki, and C. Y. Tsui, "Single inductor multiple-input multiple-output switching converter and method of use," Aug. 14 2007, US Patent 7, 256, 568.

[54] S. S. Amin and P. P. Mercier, "MISIMO: A multi-input single-inductor multi-output energy harvester employing event-driven MPPT control to achieve 89% peak efficiency and a 60000x dynamic range in 28nm FDSOI," in *2018 IEEE International Solid State Circuits Conference (ISSCC)*, Feb 2018, pp. 144–146.

[55] C. Liu, H. Lee, P. Liao, Y. Chen, M. Chung, and P. Chen, "Dual-source energy-harvesting interface with cycle-by-cycle source tracking and adaptive peak-inductor-current control," *IEEE Journal of Solid-State Circuits*, pp. 1–10, Oct. 2018.

[56] Y.-J. Ren and K. Chang, "5.8-GHz circularly polarized dual-diode rectenna and rectenna array for microwave power transmission," *IEEE Trans. Microw. Theory Techn.*, vol. 54, no. 4, pp. 1495–1502, Apr. 2006.